Research Square

Preprints are preliminary reports that have not undergone peer review.
They should not be considered conclusive, used to inform clinical practice,
or referenced by the media as validated information.

Mechanistic Analysis of NHS Mutation in Congenital Cataract via Patient-Derived hiPSC Model

Fan Fan
Eye & ENT Hospital of Fudan University
Xiaolei Lin
Shanghai Eye Diseases Prevention &Treatment Center/ Shanghai Eye Hospital, School of Medicine, Tongji University
Hongzhe Li
National Clinical Research Center for Ocular Diseases, Eye Hospital, Wenzhou Medical University
Tianke Yang
Department of Ophthalmology, The First Affiliated Hospital of USTC, Division of Life Sciences and Medicine, University of Science and Technology of China
Xin Liu
Eye & ENT Hospital of Fudan University
Yanwen Fang
Eye & ENT Hospital of Fudan University
Yi Luo
yi.luo@fdeent.org
Eye & ENT Hospital of Fudan University
Xiangjia Zhu
Eye & ENT Hospital of Fudan University

Research Article

Keywords: congenital cataracts, NHS, hiPSC, CRISPR/Cas9, ECM, ITGA2

Posted Date: August 3rd, 2026

DOI: https://doi.org/10.21203/rs.3.rs-9300845/v1

License: This work is licensed under a Creative Commons Attribution 4.0 International License.
Read Full License

Additional Declarations: No competing interests reported.

Abstract

Purpose

To clarify the functional role of Nance-Horan syndrome (NHS) gene in congenital cataract (CC) and its underlying pathogenic mechanism, focusing on lens epithelial cells (LECs) homeostasis.

Methods

NHS knockdown was performed in SRA01/04 human LECs, followed by transcriptomic, cytoskeletal, and functional analyses. Key downstream targets were validated via gain/loss-of-function assays. Urine-derived human induced pluripotent stem cells (hiPSCs) from an NHS-mutant CC patient were generated, and isogenic gene-corrected controls were established using CRISPR/Cas9. hiPSCs were differentiated into LECs for phenotypic validation.

Results

NHS depletion in SRA01/04 cells disrupted F-actin organization, reduced ZO-1 expression, impaired proliferation/migration, dysregulated cell cycle, and increased apoptosis. Transcriptomics identified enriched ECM-receptor interaction pathways, with integrin α2 (ITGA2) as a key downregulated gene. ITGA2 knockdown phenocopied NHS depletion, while NHS/ITGA2 overexpression partially rescued defects. NHS-mutant hiPSC-derived LECs exhibited cytoskeletal/junctional abnormalities, which were reversed in gene-corrected cells.

Conclusions

NHS regulates LEC homeostasis via ITGA2-mediated ECM-cytoskeleton signaling. This study establishes the first urine-derived hiPSC model of NHS-associated CC, providing mechanistic insights for targeted therapeutic development.

INTRODUCTION

Congenital cataract (CC) disease is the most common cause of preventable childhood blindness, accounting for approximately 10–35% of pediatric cases worldwide.[1–4] Pathologically, CC results from disruption of the lens microstructure and impaired function of lens-specific proteins.[5] The disease exhibits substantial hereditary and phenotypic heterogeneity.[6–8] To date, approximately 350 genes have been implicated in CC (CAT MAP; http://catmap.wustl.edu), including those encoding crystallin, gap junction proteins, membrane transporters, ion channel proteins, cytoskeletal proteins, and transcription factors.[9] Among these, mutations in the Nance–Horan syndrome (*NHS*) gene are a significant cause of

syndromic and non-syndromic CC.[8,10–12] NHS-related cataracts have been clinically documented, but the functional role of the NHS protein in lens epithelial cells (LECs) remains poorly characterized due to the limited availability of human lens tissue and the absence of physiologically relevant disease models.

The NHS protein, which is known to plays a key role in regulating the actin cytoskeleton and cellular architecture,[13,14] is constitutively expressed in the mouse lens epithelium both prenatally and postnatally, as well as in cultured human LECs.[15] Notably, NHS interacts with Abelson-interactor (Abi) family proteins through a functional homology domain.[13] Abi proteins play key roles in actin polymerization and epithelial organization, and Abi-deficient mouse models develop lens deformation, abnormal fiber alignment, and disrupted lens sutures,[16] which is similar to the phenotype of NHS-related cataracts. Co-localization of NHS with the tight junction protein ZO-1 in cell membranes also indicates a role for NHS in regulating intercellular adhesion.[14,17] These observations suggest a functional link between NHS and cytoskeletal organization that may be disrupted in NHS-related cataracts, though direct evidence in human lens cells is limited and the precise mechanisms remain unresolved.

Integrin alpha-2 (ITGA2, also known as CD49b) is a transmembrane adhesion receptor that pairs with integrin β1 to form the α2β1 heterodimer, a major collagen-binding integrin that mediates interactions with extracellular matrix (ECM). Through binding to fibrillar collagens and other ECM components, ITGA2 plays a critical role in regulating cell adhesion, migration, survival, and mechanotransduction, as well as in maintaining tissue architecture during development.[18] In the ocular lens, the precise organization of the ECM and integrin-mediated signaling are essential for lens fiber cell differentiation, alignment, and long-term transparency. Disruption of ECM-integrin interactions impairs cytoskeletal organization and intercellular communication, leading to altered lens structure and light-scattering defects.[19] Emerging genetic and functional studies implicate aberrant ITGA2 expression or function in CC, supporting the concept that defective integrin-mediated ECM signaling contributes to abnormal lens development and early-onset lens opacification.[20–22] However, the connection between NHS and ITGA2 has not been studied.

Human induced pluripotent stem cell (hiPSC) technology provides a powerful platform for modeling inherited ocular diseases. hiPSCs retain the patient's unique genetic background and can be differentiated into specific ocular cells, enabling direct study of disease mechanisms in a controlled environment. Furthermore, urine-derived cells offer a non-invasive, patient-friendly source for iPSC generation. Pairing this system with CRISPR/Cas9 genome editing technique greatly enhances mechanistic studies: pathogenic mutations can be precisely corrected to generate isogenic control lines that differ only at the disease-causing locus. Such models eliminate confounding genetic variation and have been shown to faithfully recapitulate human ocular phenotypes, including in studies of retinoschisis and inherited retinal degeneration.[23–27] Despite these advances, hiPSC-based disease modeling for CC is limited.

In this study, we demonstrate that NHS is essential for maintaining the cytoskeletal organization, tight junction integrity, cell migration, proliferation and viability of human LECs. Loss of NHS results in broad transcriptional reprogramming and dysregulation of ECM-receptor signaling. Mechanistically, ITGA2 functions downstream of NHS and mediates key aspects of ECM-cytoskeleton coupling. By generating the first urine-derived hiPSC model of CC caused by a pathogenic *NHS* mutation, and an isogenic wild-type control line, we further confirm that *NHS* mutation leads to significant abnormalities in the morphology and structure of LECs differentiated from hiPSCs.[28] Together, these findings identify an NHS-ITGA2 signaling axis that is critical for lens epithelial homeostasis, providing mechanistic insight into the pathogenesis of NHS-associated CC and a foundation for future exploration of targeted therapeutic strategies.

MATERIALS AND METHODS

Animals and cells

Eight 4-week-old immunodeficient CB-17 SCID mice were obtained from Beijing Vital River Pharmaceutical Co. Ltd. The SRA01/04 cell line was kindly provided by Professor Dan Li of Fudan University, with its original source and establishment described previously [29]. Genetic quality assessment of SRA01/04 cells, including short tandem repeat (STR) profiling and genotyping, was performed by Biowing (Shanghai, China). To ensure cell line authenticity and comply with standard cell line authentication guidelines, STR analysis results confirmed that the cell line's STR profile matched the standard reference, excluding cross-contamination or misidentification.

Lentivirus infection

Lentivirus for NHS knockdown was designed and provided by Genepharma. The target sequences in the *NHS* gene and the control sequence are listed in Sup. Table 1. SRA01/04 cells at 40–60% confluence were infected with NHS targeting (LV-NHS) or control (LV-NC) lentivirus at a multiplicity of infection (MOI) of 100. The medium was replaced the next day. The cells were observed under inverted fluorescence microscope 48 h after infection.

RNA interference (RNAi) knockdown of NHS and ITGA2

For RNAi experiments, the targeting sequences were as follows: si-NHS, 5'-ACCUUGAACUUCCAAUUAUAC-3'; si-ITGA2, 5'-CCGGCCAGAUAGUGCUAUAU-3'; si-NC, 5'-UUCUCCGAAGGUGUCACGU-3'. SRA01/04 cells were seeded onto 24 well plate at 4×10^4 cells/well. On the next day, 15 pmol of siRNA was mixed with 25 μL OPTI-MEM for 5 min; and 1.5 μL Lipofectamine 2000 (11668-027, Thermo Fisher) was mixed with 25 μL OPTI-MEM for 5 min. The siRNA solution and Lipofectamine 2000 solution were mixed for 20 min and then added to the cells for 6 h. The medium 2000 was replaced with fresh complete medium and the cells were cultured for 48 h.

Construction of overexpression plasmids

NHS and ITGA2 overexpression plasmids were constructed using the parental lentiviral vector pLVX-mCherry-N1 (Takara Bio Inc., Catalog No. 632562), which contains a CMV IE promoter, mCherry tag, and puromycin resistance gene (Puror) for selection. Full-length human NHS CDS (4443 bp) and ITGA2 CDS (3564 bp) were chemically synthesized by Jiangsu Saisuofei Biotechnology Co., Ltd. and cloned into pLVX-mCherry-N1 via XhoI-BamHI and XhoI-ApaI restriction sites, respectively. The recombinant plasmids were transformed into *E. coli* TOP10 cells, selected with ampicillin, and verified by restriction enzyme digestion (XhoI-SmaI for NHS; XhoI-EcoRI for ITGA2) and Sanger sequencing.

For cell transduction, target cells (70–80% confluency in 6-well plates) were transfected with 2 μg of purified plasmids (A_{260}/A_{280} = 1.8–1.9) using Lipofectamine 3000 (Invitrogen) per manufacturer's instructions. Stable cell lines were obtained by selection with puromycin (2 μg/ml) for 7–10 days, and mCherry expression was confirmed by fluorescence microscopy.

RNA extraction and reverse-transcription for RNA sequencing

Total RNA was extracted using TransZol Up (ET111-01, Quanshijin Biotech.), and the purity and concentration were verified. RNA reverse transcription was performed using First Strand cDNA Synthesis SuperMix for qPCR (AU341-02, Quanshijin Biotech.) according to the manufacturer's instruction. mRNA was enriched from total RNA using oligo(dT) magnetic beads (Oligotex-dT30 Super, Takara Bio Inc., Cat. No. 9086, Japan), and transcriptome libraries were constructed with the VAHTS Universal V8 RNA-seq Library Prep Kit for Illumina according to the manufacturer's protocol. Sequencing was conducted on the Illumina NovaSeq platform with the PE150 mode.

For bioinformatics analysis, raw sequencing data were filtered using fastp (v0.20.1) to remove adapters, low-quality reads (3' end quality score < 20, remaining bases with quality score < 10), reads containing ambiguous N bases, and sequences shorter than 30 bp, yielding high-quality clean data. Clean reads were mapped to the reference genome using STAR (v2.7.7a), and read counts were quantified by FeatureCounts (v2.0.0). The transcript abundance was calculated as raw counts, FPKM, and TPM using StringTie. Differentially expressed genes (DEGs) were identified with edgeR based on a negative binomial distribution model, with the criteria of FDR < 0.05 and |log2FC| ≥ 1. GO and KEGG pathway enrichment analyses of DEGs were performed using clusterProfiler (v4.0.2) with Fisher's exact test, and the Benjamini-Hochberg (BH) method was applied for multiple testing correction (corrected p-value < 0.05).

F-actin ZO-1 immunofluorescence staining

Cells grown on coverslips were fixed with immunostaining fixation solution (Beyotime Biotechnology) at RT for 10 min, followed by three washes with PBS. The cells were permeabilized using immunostaining permeabilization solution (Beyotime Biotechnology) for 5 min at RT and then washed three times with PBS. F-actin was visualized using tetramethylrhodamine isothiocyanate (TRITC)-labeled phalloidin

(Solarbio, Beijing, China). Diluted TRITC-phalloidin (80–200 nM) or anti-ZO-1 antibody (CN:21773-1-AP, Proteintech; 1:200) was prepared in PBS (pH 7.4) containing 1% immunostaining block solution (Beyotime Biotechnology) and added to the coverslips in the dark for 30 min at RT. The samples were then rinsed three times with PBS. Nuclei were counterstained with 5 μg/mL Hoechst33258 (1 μg/mL stock solution; Beyotime Biotechnology) for 1 min and subsequently washed with PBS three times. The coverslips were mounted onto slides using Fluoromount-G aqueous mounting medium (Beyotime Biotechnology). The cells were then imaged using a fluorescence or confocal microscope with excitation/emission wavelengths of 545/570 nm for TRITC-phalloidin and 364/454 nm for Hoechst.

Cell viability assay (CCK-8)

Cells cultured in 96-well plates were incubated with 10 μL of CCK-8 solution per well (CCK-8 cell proliferation/toxicity detection kit, Dojindo, Japan) for 2 h at 37°C. The optical density at 450 nm was measured using a microplate reader. Readings for LVNHS (“As”), LVNC (“Ac”), and blank control (“Ab”) cells were recorded. Cell viability was calculated using the following formula: Cell viability = [(As − Ab)/(Ac − Ab)]×100%.

Cell cycle analysis and apoptosis determination

SRA01/04 cells infected with LVNHS or LVNC were harvested and fixed in pre-chilled 70% (v/v) ethanol. The fixed cells were resuspended in 500 μL of propidium iodide (PI) staining solution and gently mixed, then incubated in the dark in a 37°C water bath for 30 min. Prior to analysis, the samples were filtered through a 40 μm cell strainer to remove aggregates. The cell cycle distribution was measured using a flow cytometer with an excitation wavelength of 488 nm. The data were analyzed using FlowJo (FlowJo vX0.7, BD) software.

Cell migration assay

Cell migration was assessed using the ibidi Cell Migration Insert Kit according to the manufacturer’s instructions. Culture inserts was positioned in 12-well plates using micro-eye surgery forceps. A total of 70 μL of cell suspension (3×10^5 cells/mL) was added to each of the two wells of the insert. After 24 h of incubation, the middle insert was gently removed horizontally to create a uniform cell-free gap. The plates were placed in a live-cell imaging workstation, and cell migration was recorded every 2 h for 24 h. The migration rate was quantified using the Area Measurement function in ImageJ software (ImageJ 1.47, NIH). The migration rate was calculated as: migration rate = (At0 − At12)/12, where At0 and At12 represent the cell-free area at 0 h and 12 h, respectively.

Cell migration was further assessed using a Transwell chamber assay. Briefly, SRA01/04 cells were harvested, resuspended in serum-free medium, and seeded into the upper chamber of Transwell chambers with 8-μm pore size membranes (TCS003024, Jiete Bio. Guangzhou, China). Complete culture

medium containing 10% fetal bovine serum was added to the lower chamber as a chemoattractant. After incubation at 37°C for 36 h, the Transwell chambers were removed, and the cells were fixed with 4% paraformaldehyde and stained with crystal violet. Non-migrated cells and non-specifically bound dye on the upper chamber surface were gently removed with a cotton swab. Migrated cells were imaged under a light microscope.

Clinical patient information

This study was conducted in accordance with the Declaration of Helsinki and was approved by the Ethics Committee of the Eye and Ear, Nose, and Throat Hospital of Fudan University (Ethics Approval No.2020076). Written informed consent was obtained from all participants or their legally authorized representatives for genetic counseling, molecular genetic testing, and collection of samples for research purposes. All experiments involving human cells derived from the patient's urine samples complied with the guidelines of the ARVO Best Practices for Using Human Eye Tissue in Research (November 2021). The primary patient, a male infant, was diagnosed with CC disease at 6 months of age. DNA sequencing and subsequent bioinformatics analyses identified a pathogenic mutation in the *NHS* gene (Table 1). The patient's urine sample was collected at 26 months of age, with no evidence of renal disease or urinary tract infection.

Table 1
Summary of high-throughput next generation sequencing results from the patient.

Item	Description
Gene	NHS
Ref. seq	NM_001291867.2
Nucleotide mutation	c.2774_2775dup
Amino acid mutation	p.Gln926Leufs*3
Gene subregion	Ex7/CDS7
Hemizygous	Hemi/Het
Location on chromosome	chrX:17726879:C > CC
Mutation type	Likely pathogenic

Urine sampling and cell culture

Midstream urine samples (≥ 100 mL) were collected under sterile conditions and mixed 1:1 with working buffer solution (UrinEasy Urine Cell Isolation and Culture Kit, Cellapy, Beijing, China). Samples were stored at 2–8°C for up to 4 h and then centrifuged at 300× *g* for 5 min. Cell pellets were resuspended in UrinEasy Isolation Complete Medium and incubated in a 37°C 5% CO_2 incubator at day 0 (D0). After the

cells adhered (typically between D4 and D7), the medium was switched to UrinEasy Urine Cell Amplification Complete Medium (UrinEasy Urine Cell Amplification and Culture Kit, Cellapy). The cells were passaged when the culture reached near-confluence. The first passage (P1) and was performed within 14 days. Subsequently, the cells were passaged every 3–4 days.

Generation of hiPSCs from urine epithelial cells

hiPSC generation from urine-derived epithelial cells was performed according to the instructions of the Reproeasy Sendai Virus hiPSC Reprogramming Kit (Cellapy). A 96-well plate was coated with Matrigel human embryonic stem cell-qualified Matrix (Corning), and the urine-derived epithelial cells were seeded at 5,000–15,000 cells per well. The next day (D0), Reprogramming Culture Medium B was added. The cell morphology was monitored daily. When early reprogramming changes (such as enlarged nucleoli) became apparent, the medium was replaced with Reprogramming Culture Medium A. On D3–4, the cells were transferred to a 6-well plate using Reprogramming Culture Medium C to ensure single-cell attachment. After the cells adhered firmly (on D4-5), the medium was replaced with fresh somatic cell culture medium. When small colony clusters (≥ 4 cells) appeared (on D5-6), the medium was switched to Reproeasy Human Cell Reprogramming Medium (Cellapy). As the colonies expanded to more than 10 cells (on D7–9), the medium was changed to PSCeasy Human Pluripotent Stem Cell Culture Medium (Cellapy). When an individual colony grew to occupy the field of view under a 10× microscope (on ~D22), it was manually picked and transferred to a Matrix-coated 48-well plate containing PSCeasy Human Pluripotent Stem Cell Recovery Medium. After cell attachment, the medium was replaced with PSCeasy Human Pluripotent Stem Cell Culture Medium, and the cells were expanded to the required passages.

Immunofluorescence staining of pluripotency markers

hiPSCs were fixed, permeabilized, and blocked under standard conditions. Primary antibodies against OCT4 (sc-9081, Santa Cruz Biotechnology), Nanog (sc293121, Santa Cruz Biotechnology), TRA-1-60, and SSEA4 (sc-21704, Santa Cruz Biotechnology) were diluted 1:100 in blocking solution and incubated with cells overnight at 4°C. Fluorescent secondary antibody (Alexa Fluor® 488 goat anti-mouse IgG (H + L), Life Technologies) was diluted 1:200 in blocking solution and applied in the dark at room temperature (RT) for 1 h. Slides were mounted using anti-fluorescence-quenching (DAPI) mounting medium (P0131, Beyotime Biotechnology, Shanghai, China). Stained cells were observed under a fluorescence microscope.

Karyotype analysis

Cells were treated with 50 ng/mL colchicine (Sinopharm, Beijing, China) for 6–8 h at 37°C and then harvested by trypsinization, resuspended in hypotonic KCl prewarmed to 37°C, and incubated at 37°C for 30 min. Next, they were fixed in 3:1 methanol:glacial acetic acid at 4°C overnight, dropped on cover slip, parched in a 75°C oven for 1–2 h, stained with Giemsa solution (Sinopharm) for 5 min, and observed under microscope. Images were analyzed using software for karyotyping and G-banding.

Teratoma formation assay

All animal experiments adhered to the ARVO Statement for the Use of Animals in Ophthalmic and Vision Research and were approved by the Institutional Animal Care and Use Committee of Fudan University (Approval No. 2020068). The teratoma assay was performed in collaboration with Peking CELLAPY Biotechnology Co., Ltd. under the same approved ethical protocol. Briefly, 5×10^6 P10 hiPSCs or H9 embryonic stem cells (control) were injected subcutaneously into both buttocks of immunodeficient CB-17 SCID mice. At two months after injection, the mice were sacrificed and the teratomas were excised, fixed, dehydrated, embedded, sectioned, deparaffinized, rehydrated, stained with hematoxylin and eosin (Huayueyang, Beijing, China), and mounted for histological evaluation under a light microscope. For the injection procedure, mice were anesthetized via intraperitoneal injection of 2% pentobarbital sodium (50 mg/kg body weight) to minimize pain and distress. After 2 months, mice were humanely euthanized by intraperitoneal administration of an overdose of pentobarbital sodium (150 mg/kg body weight). Death was confirmed by the permanent cessation of heartbeat and respiration, accompanied by the loss of pedal reflex, prior to tissue harvesting. All animal experiments described in this study were reported in compliance with the ARRIVE guidelines 2.0.

Single nucleotide polymorphism genotyping

Genomic DNA was extracted according to the manufacturer's protocol (Blood/Tissue Cell DNA Extraction Kit, Tiangen, Beijing, China). Primers flanking the NHS mutation site were used for PCR amplification: M20825-F: *TGAGGAAGTCTGATGGAAACG*; M20825-R: *GGAGCCAGAGGTCTGCA*. The PCR products were analyzed by 1% agarose gel electrophoresis and sequenced by Genewiz. According to the ACMG/AMP variant interpretation guidelines (2015), the identified NHS mutation (c.2774_2775dup, p.Gln926Leufs*3) was classified as 'likely pathogenic' based on the following criteria: protein truncation leading to loss of function (PVS1), extremely low frequency in general population databases (PM2), and phenotypic co-segregation with congenital cataract (PP1).

CRISPR/Cas9 editing of hiPSCs

Single-guide RNA (sgRNA) was synthesized using the GeneArt Precision gRNA Synthesis Kit (A29377, Thermo Fisher Scientific) targeting the sequence ATCCGAAGCATCTAACTGAG near the *NHS* c.2773C > CCT mutation site, designated as sgNHS#1. hiPSCs were cultured in mTeSR1 medium (05850, StemCell) and maintained at 37°C with 5% CO_2. A single-stranded donor oligonucleotide, corresponding to the sgRNA target and designated NHS-donor #1, was designed and synthesized for homology-directed repair, with the following sequence:
AACACGCCTTCTCGAATGGAAAACGCCAATCTTCCCACCAAGCAGGAACCTTCT
TGGATAAACCAGAGTGAACAAGGCATTAAGGAACCTCAGTTAGATGCTTCGGATATT
CCACCATTCAA (the corrected nucleotide is highlighted in red).

The sgRNA/Cas9 ribonucleoprotein complex (Invitrogen TrueCut Cas9 Protein v2, A36498, Thermo Fisher Scientific) and single-stranded donor oligonucleotide were delivered into hiPSCs via electroporation (Neon® Transfection System Kit, MPK1096, Thermo Fisher Scientific). Two to three days post-transfection, a subset of cells was harvested for sequencing analysis. Genomic DNA was extracted

using the Cell Genomic DNA Extraction Kit (KR008A, Youcheng, Ningbo, China) according to the manufacturer's instructions. The target region was amplified by PCR using the following primers: NHS-F: AATGAAGCTGCCTCTTGATTTC and NHS-R: ATCAATGACTGTGGTACCCGTAC. The PCR product was subjected to Sanger sequencing by Genewiz to verify the correction of the *NHS* mutation.

Directed differentiation of hiPSCs

According to the lentoid body differentiation protocol described by Fu *et al*.[28], differentiation of hiPSCs into LECs was induced using a three-stage method involving sequential culturing in different combinations of growth factors. Recombinant human proteins hNoggin (CV89, Novoprotein), hFGFb (C779, Novoprotein), hBMP-7 (120-03p-10, Pepro Tech), and hBMP-4 (120-05-5, Pepro Tech) were dissolved in the manufacturer recommended solvents (sterile water or citric acid solution) to a stock concentration of 100 μg/mL. Recombinant WNT-3a (5036-WN-010, R&D) was dissolved in PBS to a stock concentration of 100 μg/mL. All proteins were aliquoted and stored at − 20°C. Solutions were prepared freshly and were used within one week. Two vials of frozen hiPSCs were thawed and expanded under standard culture conditions. The cells were maintained at a density of 20 − 40% prior to the initiation of differentiation. The first day of transition to the directed differentiation medium was designated as Day 0 (D0).

Stage I differentiation (D0–D5) was initiated using PSCeasy medium (50 mL) supplemented with hNoggin (50 μL-final concentration of 100 ng/mL). Fresh medium was added daily. Cells harvested on D5 were transferred into 96-well suspension culture plates at a density of 1×10^5 cells/well to form the lentoid bodies.

For Stage II differentiation (D6–D14), cells were cultured in PSCeasy medium (50 mL) supplemented with hFGFb (50 μL-final concentration of 100 ng/mL) and hBMP-4/7 (10 μL-final concentration of 20 ng/mL). The medium was replaced daily without passaging. Care was taken to avoid disturbing or aspirating the forming embryoid bodies. Between D10 and D13, the cells progressively developed lamellar structures surrounding the colonies, producing characteristic "rose-like" or "fried-egg-like" morphology. When the cell culture approached full confluence, the central lamellar region ("flower core" or "yolk") was removed using a sterile 200 μL pipette tip under microscope in a biosafety cabinet. The cells were subsequently passaged at a 1:4 to 1:6 ratio.

For Stage III differentiation (D15–D25), the cells were maintained in PSCeasy medium (50 mL) supplemented with WNT-3a (5 μL-final concentration of 20 ng/mL) and hFGFb (50 μL-final concentration of 100 ng/mL). The medium was replaced daily. During this stage, the cells approached terminal differentiation and were passaged at a 1:3 ratio as needed.

Real-time qPCR

Total RNA was extracted using the TRIzol (Invitrogen) method. The RNA purity and concentration were verified prior to downstream analysis. cDNA was synthesized using a PrimeScript RT Reagent Kit (RR037A, Takara), and real-time quantitative PCR (qPCR) was performed using a QuantiNova SYBR

Green PCR kit (Qiagen). Gene-specific primers were designed and synthesized by Gima Gene Biotech Co. (Sup. Table 2). GAPDH was used as the internal control gene. Relative mRNA expression levels were determined using the $2^{-\Delta\Delta Ct}$ method. All reactions were performed in triplicate, and mean values were used for analysis.

Statistical Analyses

Statistical analyses were performed using GraphPad Prism 8.0. Unless otherwise specified, all quantitative data are presented as mean ± standard deviation (SD) from three independent biological replicates (n = 3). Comparisons between two groups were conducted using an unpaired *t*-test. When normality or homogeneity of variance assumptions were not met ($P < 0.05$), the nonparametric Mann-Whitney test was used. Differences were considered statistically significant at $P < 0.05$.

RESULTS

NHS Knockdown Disrupts the Cytoskeletal/Junctional Structure in SRA01/04 LECs

To investigate the intracellular function of NHS in LECs, we performed knockdown experiments in the human LEC line SRA01/04, a widely used model for cataract and ocular research. SRA01/04 cells were infected with GFP-lentiviruses expressing either NHS-targeting shRNA (LV-NHS) or scrambled control RNA (LV-NC). At a MOI of 100, the cells achieved ≥ 80% infection efficiency (Sup. Figure 1A). RT-qPCR analysis confirmed that NHS expression was significantly reduced in the LV-NHS group compared to controls (Sup. Figure 1B). Four days post-infection, SRA01/04 cells with NHS knockdown exhibited marked morphological changes, including cell enlargement, irregular shape, dispersed cytoplasm, and enlarged fragmented nuclei. In contrast, cells infected with LV-NC maintained a morphology similar to that of untreated SRA01/04 cells (Fig. 1A).

To determine whether knockdown of NHS expression affects F-actin, we performed staining assays with TRITC-labeled Phalloidin derivatives. Compared with LV-NC infected cells, LV-NHS infected SRA01/04 cells exhibited a pronounced reduction in F-actin content (Fig. 1B), indicating that NHS plays a crucial role in maintaining cytoskeletal organization and actin filament content. Immunofluorescent staining also revealed robust ZO-1 expression at intercellular contacts in SRA01/04 and LV-NC cells, with markedly reduced ZO-1 levels and disrupted protein localization in LV-NHS cells (Fig. 1C). These results suggest that NHS is closely associated with the normal morphology of LECs, including the cytoskeletal structure and tight junction protein expression and organization.

NHS Regulates Cell Proliferation, Migration, and Cell Cycle Progression

To determine whether NHS knockdown affects the proliferation of SRA01/04 cells, we performed CCK-8 assays. LV-NHS-infected SRA01/04 cells exhibited significantly reduced proliferative capacity and lower cell viability compared with LV-NC-infected control cells (Fig. 2A, B). We also monitored cell migration dynamically using an ibidi cell migration insert and a 24-hour live-cell imaging workstation. Quantitative analysis with ImageJ demonstrated a marked decrease in the migration ability following NHS knockdown (P = 0.0004) (Fig. 2C). Finally, we evaluated cell cycle progression by PI staining of dsDNA followed by flow cytometry (Fig. 2D). Lentiviral infection itself caused modest changes, including a more dispersed S-phase population and a slight decrease in the G2/M peak. In contrast, NHS knockdown induced profound effects: G0/G1 phase cells were largely absent, indicating cell cycle arrest, accompanied by a significantly increased apoptotic cell population. These results suggest that NHS is essential for maintaining normal cell proliferation, migration, and cell cycle progression in LECs.

NHS-Dependent ITGA2 Expression Regulates Cell Viability, Migration, and Cell Cycle Progression

To explore the effects of NHS knockdown, we transfected SRA01/04 cells with si-NC (scrambled control siRNA) and si-NHS (Sup. Figure 2A). A total of 1311 DEGs were identified, including 411 up-regulated and 900 down-regulated DEGs (Sup. Figure 2B). NHS knockdown resulted in broad transcriptomic reprogramming, suggesting that NHS is functionally important for maintaining the transcriptional state of LECs. Hierarchical clustering heatmap (Z-score) analysis of DEGs revealed clear segregation of the samples, indicating good intra-group consistency and distinct transcriptional profiles between si-NC and si-NHS cells (Sup. Figure 2C). GO annotation showed that the DEGs were enriched in functions related to nuclear division, chromosome segregation, positive regulation of cell cycle, collagen-containing extracellular matrix, spindle, microtubule, apical part of cell, synaptic membrane, ion channel activity, passive transmembrane transporter activity, actin binding, tubulin binding microtubule binding, ECM structural constituent, *etc.* (Sup. Figure 2D). Furthermore, KEGG analysis revealed enriched pathways, including ECM-receptor interaction, cell adhesion molecules, cholinergic synapse, neuroactive ligand-receptor interaction, *etc.* (Sup. Figure 2E).

The core function of the ECM-receptor interaction pathway is to connect the ECM with the intracellular cytoskeleton (especially actin) through receptors such as integrins, thereby regulating cytoskeleton assembly, cell junction stability, and cell morphology maintenance. Therefore, given our results indicating that DEGs in this pathway are enriched in NHS knockdown cells, we evaluated effects on the expression of several members of this pathway (*ITGA2, ITGA11, ITGA7, TNXB*, and *HMMR*) (Sup. Figure 3). qPCR results demonstrated that the expression of *ITGA2* and *ITGA11* showed a significant decrease in si-NHS cells compared to si-NC control cells, which is consistent with the RNA sequencing results. Because *ITGA2* demonstrated the most significant decrease, it was selected for further study. The following SRA01/04-derived cell lines were constructed: si-ITGA2 (ITGA2 knockdown), si-ITGA2 + OE-NHS (ITGA2 knockdown with NHS overexpression), si-ITGA2 + OE-NC (ITGA2 knockdown with overexpression control), si-NHS, and si-NHS + OE-ITGA2 (NHS knockdown with ITGA2 overexpression) (Sup. Figure 4A–C). CCK-8 assays showed that si-ITGA2 cells exhibited significantly reduced cell viability compared with

siNC control cells (Fig. 3A). Furthermore, overexpression of NHS in si-ITGA2 + OE-NHS cells rescued the cell viability phenotype compared with the si-ITGA2 and si-ITGA2 + OE-NC cells (Fig. 3A). In a reciprocal experiment, overexpression of ITGA2 in si-NHS + OE-ITGA2 cells also rescued the cell viability decrease caused by NHS knockdown (Fig. 3B).

To further evaluate the effects of NHS-dependent ITGA2 expression on migration, we performed Transwell assays. The results showed that migrated cell number was markedly decreased in si-ITGA2 cells, while the addition of the NHS over-expression vector (si-ITGA2 + OE-NHS), but not the control over-expression vector (si-ITGA2 + OE-NC), rescued the migration to wild-type levels (Fig. 3C). Similarly, overexpression of ITGA2 in NHS knockdown cells (si-NHS + OE-ITGA2) compared with si-NHS cells increased cell migration (Fig. 3D).

Next, we evaluated the effects of NHS-dependent ITGA2 expression on cell cycle progression. Compare with si-NC control cells, si-ITGA2 cells had a statistically significantly decreased proportion in G0/G1 phase and increased proportion in G2/M and S phases. Interestingly, overexpression of NHS (si-ITGA2 + OE-NHS) led to a further decrease in the G0/G1 proportion and a significant increase in the G2/M proportion (Fig. 3E, F). Overexpression of ITGA2 in NHS knockdown cells (si-NHS + OE-ITGA2) caused a similar phenotype, with a further decrease in G0/G1 cells and an increase in S phase cells (Fig. 3G, H). These results suggest that ITGA2 is essential for maintaining normal cell proliferation, viability, migration, and cell cycle progression in LECs, and overexpression of NHS can compensate for the cell proliferation, viability, and migration effects caused by ITGA2 depletion. Additionally, reciprocal overexpression of ITGA2 in NHS knockdown cells showed similar effects, suggesting a direct correlation between NHS and ITGA2.

To further validate the functional link between NHS, ITGA2, and the ECM-receptor interaction pathway (which connects ECM to the intracellular cytoskeleton), we performed cytoskeleton staining to assess cell spreading. As shown in Fig. 3I, si-NC control cells exhibited normal spreading with a well-developed cytoskeleton, while si-ITGA2 cells displayed a reduction in the cell surface area. Notably, overexpression of NHS in si-ITGA2 + OE-NHS cells rescued and even increased the cell surface area compared to those of si-ITGA2 cells, whereas the control overexpression vector (si-ITGA2 + OE-NC) failed to reverse this phenotype. In reciprocal experiments (Fig. 3J), si-NHS cells showed diminished cell spreading and reduced surface area relative to si-NC controls, and this defect was effectively rescued by overexpression of ITGA2 in si-NHS + OE-ITGA2 cells.

Collectively, these results demonstrate that ITGA2 is essential for maintaining normal cell proliferation, viability, migration, cell cycle progression, and cytoskeleton-dependent cell spreading in LECs. Moreover, the ability of NHS overexpression to compensate for ITGA2 depletion, and vice versa, reflects a close functional interplay between NHS and ITGA2 within the ECM-receptor interaction pathway—supporting their coordinated regulation of these cellular processes and consistent with the enrichment of pathway-related DEGs in NHS knockdown cells.

Establishment of a urine-derived hiPSC model of CC with the NHS Mutation

To develop a physiologically relevant ex vivo model for CC based on urine-derived hiPSCs from a CC patient, we isolated urine-derived somatic cells and expanded them in culture, as shown in Sup. Figure 5. Reprogramming was performed using a Sendai virus–based system to deliver exogenous factors. From D1 onward, the cells exhibited clear morphological changes characteristic of early reprogramming, including marked nucleolar enlargement. Over time, the cells progressively transitioned from an elongated spindle-shaped morphology to a round appearance and then aggregated and expanded in clusters. The progression of morphological changes observed throughout the 22-day reprogramming period is shown in Sup. Figure 6.

To verify whether the reprogrammed urine-derived cells acquired pluripotent stem cell identity, we performed immunofluorescence staining of Nanog, OCT4, Sox2, and SSEA-4. As shown in Fig. 4A, the reprogrammed cells robustly expressed each of these pluripotency markers, confirming the successful induction of hiPSCs. To rule out chromosomal abnormalities, we performed karyotype analysis after 10 passages of the hiPSCs. G-banding analysis confirmed that the hiPSCs maintained a normal karyotype, consisting of 46 chromosomes, with sex chromosomes consistent with the donor child's sex (XY) (Fig. 4B). To further assess pluripotency *in vivo*, we performed teratoma formation assays. Reprogrammed hiPSCs were subcutaneously injected into immunodeficient CB-17 SCID mice (#6, 7, and 8) to evaluate their ability to differentiate into all three germ layers. As a control, embryonic stem cells (H9) were injected into mouse #5. One-month post-injection, subcutaneous tumors formed at the injection sites in all mice. Mice #5 and #6 were sacrificed at 2 months, while mice #7 and #8 were sacrificed prematurely at 40 days due to poor health.

The tumors were collected and weighed following sacrifice. The results demonstrate that the teratomas derived from patient-specific hiPSCs were smaller than those formed by H9 cells over the same period (Fig. 4C, Sup. Table 3). Additionally, histological examination using hematoxylin and eosin staining confirmed the presence of tissues representing all three germ layers within the teratomas: columnar epithelium from endoderm, muscle tissue from mesoderm, and neuroepithelium from ectoderm (Fig. 4D–F). These results demonstrate that the hiPSCs established in this study are chromosomally stable and capable of differentiating into all three germ layers *in vivo*.

Based on the above protocol, a hiPSC line specific to a patient with *NHS*-mutant CC (NHS-MT) was successfully established, providing a stable platform that can be reliably passaged over multiple generations. As shown in Fig. 4G, the morphology of 15th-generation cells on Days 1 and 5 after passage is comparable to that of the original (0th-generation) hiPSCs. The cells formed dense, round colonies, exhibiting a high nucleocytoplasmic ratio and minimal intercellular spacing, with growth characteristics similar to that of the parental population. To verify that the reprogrammed hiPSCs retained the patient's genetic background, single nucleotide polymorphism analysis was performed. The results confirmed that the hiPSCs preserved the same *NHS* gene mutation as the donor as observe in the high-throughput

sequencing data from the patient (data not shown), demonstrating genetic fidelity of the reprogrammed cell line.

CRISPR/Cas9-Mediated Correction of the NHS Mutation in hiPSCs

To prepare a control (GE-NHS-WT) for the NHS-MT mutation-containing hiPSC line, we performed CRISPR/Cas9. Sanger sequencing of the GE-NHS-WT hiPSCs demonstrated correction of the “c.2773C > CCT” mutation in the *NHS* gene. In the initial mixed cell population, dual peaks at the mutation site indicate the presence of both the original and corrected alleles (Sup. Figure 7A). The mixed population was expanded, single colonies were isolated, and the target DNA was sequenced. Colonies harboring the corrected *NHS* sequence were identified after the first round of screening. To further enhance the purity of the correct clones, one of these colonies underwent a second round of single-colony expansion and genotyping. All six colonies screened in the second round exhibited the corrected sequence (Sup. Figure 7B), confirming successful CRISPR/Cas9-mediated gene correction. After clonal expansion, a third round of sequencing confirmed the identity and purity of the edited hiPSCs, demonstrating that the GE-NHS-WT control hiPSC line with the corrected *NHS* mutation was successfully established at 100% purity.

hiPSCs Differentiation into LECs

To induce differentiation of hiPSCs into LECs, we employed a three-stage chemical induction protocol.[28] Morphological changes in adherent hiPSCs became apparent 10–13 days after initiation of differentiation. The cells elongated into a spindle shape and were organized into characteristic rose wreath–like structures, forming a single layer with tightly packed cells and well-defined boundaries between wreaths (Fig. 5A). During the first stage of differentiation in suspension culture (D2), hiPSCs began forming embryoid bodies, which gradually increased in size. Semi-spherical small embryoid bodies also formed on the periphery of the original clusters. By D25, tissue clusters of approximately 2 mm in diameter were observed. No obvious morphological differences were noted between tissue clusters derived from NHS-MT and GE-NHS-WT cells (Fig. 5B, C). E-cadherin, an epithelial cell marker, as well as CRYAA and CRYB, which are lens-specific markers, were positive in the differentiated cells (Fig. 5D), indicating successful differentiation. These results demonstrate the repeatability and effectiveness of the three-stage differentiation protocol, thus verifying that urine-derived hiPSCs can be successfully differentiated into LECs.

Differentiated NHS-MT Cells Exhibit Cytoskeletal and Junctional Defects

Our above results show that knockdown of NHS in SRA01/04 cells led to pronounced morphological and physiological defects. To determine whether similar defects occur in hiPSC-derived LECs, we performed immunofluorescent staining analysis of ZO-1 and F-actin in differentiated NHS-MT and GE-NHS-WT cells. The results revealed that the ZO-1 distribution at the cell peripheries was dispersed and irregular in NHS-MT cells, in contrast to the abundant and well-defined ZO-1 localization in gene-edited, corrected GE-NHS-WT cells (Fig. 6A). Although overall F-actin protein levels were not significantly different between

NHS-MT and GE-NHS-WT cells, F-actin organization in NHS-MT cells was irregular and disrupted (Fig. 6B), recapitulating the cytoskeletal phenotypes observed in NHS knockdown SRA01/04 cells. These findings indicate that the *NHS* mutation impairs the cytoskeletal and junctional organization in differentiated LECs.

DISCUSSION

In this study, we demonstrated that NHS plays a central role in maintaining the structural integrity, proliferative capacity, and functional homeostasis of human lens epithelial cells. Using both an established LEC line and a patient-derived hiPSC model of congenital cataract caused by a pathogenic *NHS* mutation, we show that loss of NHS function leads to profound defects in cytoskeletal organization, tight junction integrity, cell proliferation, migration, and cell cycle progression, which are essential for normal lens development and transparency.

Our initial NHS knockdown experiments in SRA01/04 cells revealed that depletion of NHS resulted in striking morphological abnormalities, including cell enlargement, nuclear fragmentation, and cytoplasmic dispersion. These changes were accompanied by a pronounced reduction in the F-actin content and disrupted localization of the tight junction protein ZO-1, indicating compromised cytoskeletal and junctional architecture. Given the critical role of actin and intercellular junctions in maintaining lens epithelial polarity and barrier function, [30–33] these findings provide a direct cellular explanation for how NHS deficiency may predispose patients to lens opacification.

Beyond the structural defects, NHS knockdown significantly impaired LEC proliferation and migration and caused severe cell cycle abnormalities. These phenotypes are consistent with the extensive transcriptional reprogramming observed upon NHS depletion, as revealed by RNA sequencing analysis. Notably, the DEGs were enriched in biological processes related to nuclear division, spindle organization, microtubule dynamics, and actin binding, underscoring the broad impact of NHS on cytoskeletal and cell cycle regulation. One of the most significant findings of our transcriptomic analysis was the enrichment of the ECM-receptor interaction pathway among DEGs. This pathway serves as a key interface linking ECM components to the intracellular cytoskeleton through integrins, thereby regulating cell shape, adhesion, migration, and mechanotransduction.[18] Disruption of this pathway provides a compelling mechanistic framework to explain the observed cytoskeletal and junctional abnormalities following *NHS* knockdown. Among ECM-receptor interaction genes, *ITGA2* exhibited the most pronounced downregulation and was therefore selected for further functional analysis.

Our loss- and gain-of-function studies demonstrated that *ITGA2* is essential for maintaining normal proliferation, viability, migration, and cell cycle progression in LECs. Knockdown of ITGA2 recapitulated many of the defects observed upon NHS depletion, while overexpression of NHS in ITGA2-deficient cells substantially rescued the cell viability and migratory capacity. Conversely, overexpression of ITGA2 in NHS knockdown cells similarly restored key cellular functions. Cell cycle analysis shows that while NHS/ITGA2 knockdown disrupted normal G1 progression, overexpression of ITGA2/NHS failed to restore

the cell cycle distribution, suggesting that NHS and ITGA2 may regulate cell cycle progression through overlapping but non-identical mechanisms. These reciprocal rescue experiments strongly support a functional and mechanistic link between NHS and ITGA2, suggesting that NHS may regulate lens epithelial homeostasis, at least in part, through modulation of integrin-mediated ECM-cytoskeleton signaling.

To extend our findings beyond immortalized cell lines, we established a patient-specific, urine-derived hiPSC model carrying a CC-associated *NHS* mutation and generated an isogenic gene-corrected control using CRISPR/Cas9. Differentiation of these hiPSCs into LECs revealed that *NHS*-mutant cells exhibited disrupted F-actin organization and aberrant ZO-1 localization, closely mirroring the phenotype observed in NHS knockdown SRA01/04 cells. Importantly, these defects were rescued in the gene-corrected GE-NHS-WT LECs, providing genetic evidence that the observed abnormalities are directly attributable to the *NHS* mutation rather than inter-individual variability. The CRISPR/Cas9 system has been shown to exhibit superior genome-editing efficiency in stem cells compared with other gene-editing methods, and combining CRISPR/Cas9 with hiPSC technology enables the construction of highly precise, personalized disease models.[35–40] Therefore, by correcting the mutation in the hiPSC line using CRISPR/Cas9, our study establishes a powerful and reproducible platform for further mechanistic studies, drug screening, or therapeutic development.

Notably, our results demonstrate that urinary cells can serve as a practical and noninvasive source for generating hiPSCs from pediatric patients with hereditary diseases. Traditionally, hiPSCs are generated from somatic cells obtained from skin or peripheral blood. In 2011, researchers in China successfully established hiPSCs for the first time using urine-derived cells.[41] Because urine collection is convenient, noninvasive, and cost-effective, it has become an attractive source of somatic cells for hiPSC generation. In this study, we collected urine samples from a child with CC and generated hiPSCs using a non-integrating Sendai virus system under a feeder-free, KSR-free culture condition.[42–44] The patient-specific hiPSCs retained the *NHS* mutation and the patient's genetic background, providing a robust cellular model for subsequent mechanistic analysis. The successful differentiation of these hiPSCs into LECs further validates the usefulness of this system for modeling developmental defects.

Together, our data support a model in which NHS functions as a key regulator of cytoskeletal organization and cell-cell junction integrity in LECs, acting upstream of ECM-integrin signaling pathways involving *ITGA2*. Disruption of this regulatory axis compromises lens epithelial structure, proliferation, and survival, thereby contributing to abnormal lens development and congenital cataract formation. These findings provide mechanistic insight into the pathogenesis of congenital cataract and highlight the broader importance of ECM-cytoskeleton coupling in maintaining lens transparency. Future studies aimed at defining the precise molecular interactions between NHS, integrins, and actin-regulatory complexes may uncover novel therapeutic targets for congenital cataracts and related lens disorders.

Abbreviations

CC
congenital cataracts
ECM
extracellular matrix
hiPSCs
human induced pluripotent stem cells
iPSC
induced pluripotent stem cell
ITGA2
integrin α2
LECs
lens epithelial cells
MOI
multiplicity of infection
NHS
Nance-Horan Syndrome
OE
overexpression
PI
propidium iodide
qPCR
realtime quantitative PCR
RT
room temperature
sgRNA
single-guide RNA
SSEA
stage-specific embryonic antigens
STR
short tandem repeat
TRITC
tetramethylrhodamine isothiocyanate

Declarations

Funding This work was supported by the National Natural Science Foundation of China (Grant No. 82201162 and 81870645).

Conflict of Interest The authors declare no financial or non-financial interests that could be perceived as influencing the work reported in this manuscript.

Ethics approval and consent to participate

The SRA01/04 human lens epithelial cell line was kindly provided by Professor Dan Li of Fudan University. The original cell source has formally confirmed that the collection of original human samples for establishing this cell line was conducted with valid prior ethical approval, and all corresponding cell donors have signed written informed consent forms before sample collection.The cells were obtained and used in accordance with the Material Transfer Agreement (MTA) between the provider and our institution, and the cell line was characterized as described in the original publication.[29] The identity of the SRA01/04 cell line was verified via short tandem repeat (STR) authentication by Biowing Biotechnology Co., Ltd. (Shanghai, China).

Patient-derived induced pluripotent stem cells (iPSCs) were reprogrammed from human urine samples collected under a formally approved ethical research protocol. Written informed consent was mandatorily obtained from the legal guardian of the urine donor prior to sample collection and subsequent iPSC generation.

For the clinical patient-related study involved in this work: this study was reviewed and approved by the Ethics Committee of the Eye & ENT Hospital of Fudan University. The full approved project title is Genetic Mechanisms and Functional Studies of Congenital Cataract, with an official approval number of 2020076, and the approval date was August 2020. All enrolled patients or their legal guardians provided signed written informed consent before participating in this clinical research and allowing the usage of their biological samples for experimental analysis.

For all animal experiments performed in this study: all in vivo animal operations and experimental protocols were reviewed and approved by the Institutional Animal Care and Use Committee of Fudan University. The full approved animal project title is Regulatory Mechanisms of the Pro-inflammatory Cytokine MCP-1 on Intraocular Microinflammation in High Myopia-Associated Cataract, with an official approval number of 2020068, and the approval date was February 2020. All animal experimental procedures strictly complied with the ARRIVE guidelines and national laboratory animal welfare regulations.

Data Availability Statement

The high-throughput RNA-sequencing datasets generated and analyzed during the current study are deposited and publicly available in the Genome Sequence Archive for Human (GSA-Human) at the National Genomics Data Center (NGDC), China National Center for Bioinformation (CNCB), under BioProject accession number PRJCA067549 and GSA-Human accession number HRA019336. Other raw data supporting the findings of this study are available from the corresponding author upon reasonable request.

Competing interests

The authors declare that they have no competing financial or non-financial interests associated with this work.

Author contributions FanFan: Performed the experiments, analyzed and interpreted the data and wrote the original manuscript; Xiaolei Lin: Contributed reagents, materials, analysis tools and data.; Tianke Yang: Performed the experiments. Hongzhe Li, Analyzed and interpreted the data; Yanwen Fang: responsible for cataract surgery and sample collection; XiangJia Zhu: Conceived and revised the manuscript; Yi Luo : Designed the experiments, responsible for cataract surgery and conceived the manuscript.

Acknowledgments We thank Peking CELLAPY Biotechnology Co., Ltd. for technical assistance with cell reprogramming. The authors declare that they have not used AI-generated work in this manuscript.

References

1. Wu X, Long E, Lin H, Liu. (2016) Prevalence and epidemiological characteristics of congenital cataract: a systematic review and meta-analysis. Y.Sci Rep. 2016;6:28564.
2. Solebo AL, Teoh L, Rahi J. (2017) Epidemiology of blindness in children. Arch Dis Child. 2017;102(9):853–857.
3. Daien V, Le Pape A, Heve D et al. (2010) Incidence and Characteristics of Congenital Cataract Surgery in France from 2010 to 2012: The EPISAFE Program[J]. Ophthalmic Res. 2017;58(2):114–116.
4. Sheeladevi S, Lawrenson JG, Fielder AR, Suttle CM. (2016) Global prevalence of childhood cataract: a systematic review. Eye (Lond). 2016;30(9):1160-9.
5. Wirth MG, Russell-Eggitt IM, Craig JE et al. (2002) Aetiology of congenital and paediatric cataract in an Australian population[J]. Brit J Ophthalmol. 2002;86(7):782–786.
6. Li JY, Leng YJ, Han SR et al. (2018) Clinical and genetic characteristics of Chinese patients with familial or sporadic pediatric cataract[J]. Orphanet J Rare Dis. 2018;13.
7. Wang H, Zhang LL, Wang N et al. (2018) Next-generation sequencing reveals genetic landscape in 46, XY disorders of sexual development patients with variable phenotypes[J]. Human Genetics. 2018;137(3):265–277.
8. Burdon KP, McKay JD, Sale MM, Russell-Eggitt IM, Mackey DA, Wirth MG, Elder JE, Nicoll A, Clarke MP, FitzGerald LM, Stankovich JM, Shaw MA, Sharma S, Gajovic S, Gruss P, Ross S, Thomas P, Voss AK, Thomas T, Gécz J, Craig JE. (2003) Mutations in a novel gene, NHS, cause the pleiotropic effects of Nance-Horan syndrome, including severe congenital cataract, dental anomalies, and mental retardation. Am J Hum Genet. 2003;73(5):1120-30.
9. Miller C, Gertsen BG, Schroeder AL, Fong CT, Iqbal MA, Zhang B. (2021) Allelic and dosage effects of NHS in X-linked cataract and Nance-Horan syndrome: a family study and literature review. Mol Cytogenet. 2021;14(1):48.

10. Brooks SP, Ebenezer ND, Poopalasundaram S, Lehmann OJ, Moore AT, Hardcastle AJ. (2004) Identification of the gene for Nance–Horan syndrome (NHS) J. Med. Genet. 2004;41:768–771.
11. Coccia M, Brooks SP, Webb TR et al. (2009) X-linked cataract and Nance-Horan syndrome are allelic disorders[J]. Hum Mol Genet. 2009;18(14):2643–2655.
12. Sun W, Xiao X, Li S et al. (2014) Exome sequencing of 18 Chinese families with congenital cataracts: a new sight of the NHS gene[J]. PloS one. 2014;9(6):e100455.
13. Brooks SP, Coccia M, Tang HR, Nanuga N, Machesky LM, Bailly M, Cheetham ME, Harcastle AJ. (2010) The Nance–Horan syndrome protein encodes a functional WAVE homology domain (WHD) and is important for co-ordinating actin remodelling and maintaining cell morphology. Hum Mol Genet. 2010;19(12):2421–2432.
14. Sharma S, Ang SL, Shaw M et al. (2006) Nance-Horan syndrome protein, NHS, associates with epithelial cell junctions[J]. Hum Mol Genet. 2006;15(12):1972–1983.
15. Xue C, Chu Q, Shi Q, Zeng Y, Lu J, Li L. (2025) Wnt signaling pathways in biology and disease: mechanisms and therapeutic advances. Signal Transduct Target Ther. 2025;10(1):106. 10.1038/s41392-025-02142-w.PMID: 40180907.
16. Grove M, Demyanenko G, Echarri A et al. (2004) Abi2-deficient mice exhibit defective cell migration, aberrant dendritic spine morphogenesis, and deficits in learning and memory[J]. Mol Cell Biol. 2004;24(24):10905–10922.
17. Huang KM, Wu J, Duncan MK et al. (2006) Xcat, a novel mouse model for Nance-Horan syndrome inhibits expression of the cytoplasmic-targeted Nhs1 isoform[J]. Hum Mol Genet. 2006;15(2):319–327.
18. Adorno-Cruz V, Liu H. (2018). Regulation and functions of integrin α2 in cell adhesion and disease. Genes Dis. 2018;6(1):16–24.
19. Wederell ED, de Iongh RU. (2006). Extracellular matrix and integrin signaling in lens development and cataract. Semin Cell Dev Biol. 2006;17(6):759 – 76.
20. Bell SJ, Oluonye N, Harding P, Moosajee M. (2020). Congenital cataract: a guide to genetic and clinical management. Ther Adv Rare Dis. 2020;1:2633004020938061.
21. Walker J, Menko AS. Integrins in Lens Development and Disease. Exp Eye Res. 2009;88(2):216–25.
22. Mrugacz M, Bryl A, Falkowski M, Zorena K. (2021). Integrins: An Important Link between Angiogenesis, Inflammation and Eye Diseases. Cells. 2021;10(7):1703.
23. Avior Y, Sagi I, Benvenisty N. (2016) Pluripotent stem cells in disease modelling and drug discovery[J]. Nat Rev Mol Cell Biol. 2016;17(3):170–182.
24. Lukovic D, Castro AA, Delgado ABG et al. (2015) Human iPSC derived disease model of MERTK-associated retinitis pigmentosa[J]. Sci Rep-Uk. 2015;5. ARTN 12910.
25. Ramsden CM, Nommiste B, Lane AR et al. (2017) Rescue of the MERTK phagocytic defect in a human iPSC disease model using translational read-through inducing drugs[J]. Sci Rep-Uk. 2017;7. ARTN 5110.

26. Granata A, Serrano F, Bernard WG et al. (2017) An iPSC-derived vascular model of Marfan syndrome identifies key mediators of smooth muscle cell death[J]. Nat Genet. 2017;49(1):97–109.
27. Huang KC, Wang ML, Chen SJ et al. (2019) Morphological and Molecular Defects in Human Three-Dimensional Retinal Organoid Model of X-Linked Juvenile Retinoschisis[J]. Stem Cell Reports. 2019;13(5):906–923.
28. Fu Q, Qin Z, Jin X et al. (2017) Generation of Functional Lentoid Bodies From Human Induced Pluripotent Stem Cells Derived From Urinary Cells[J]. Invest Ophthalmol Vis Sci. 2017;58(1):517–527.
29. Ibaraki N, Chen SC, LR L, et al. Human lens epithelial cell line. Exp Eye Res. 1998;67(5):577–85.
30. Kerr CL, Zaveri MA, Robinson ML, Williams T, West-Mays JA. (2014). AP-2α is required after lens vesicle formation to maintain lens integrity. Dev Dyn. 2014;243(10):1298 – 309.
31. Karnam S, Maddala R, Stiber JA, Rao PV. (2021) Drebrin, an actin-binding protein, is required for lens morphogenesis and growth. Dev Dyn. 2021;250(11):1600–1617.
32. Wever GF, Menko AS. (2006) Actin filament organization regulates the induction of lens cell differentiation and survival. Dev Biol. 2006;295(2):714 – 29.
33. Berthoud VM, Gao J, Minogue PJ, Jara O, Mathias RT, Beyer EC. (2020). Connexin Mutants Compromise the Lens Circulation and Cause Cataracts through Biomineralization. Int J Mol Sci. 2020;21(16):5822.
34. Ding QR, Regan SN, Xia YL et al. (2013) Enhanced Efficiency of Human Pluripotent Stem Cell Genome Editing through Replacing TALENs with CRISPRs[J]. Cell Stem Cell. 2013;12(4):393–394.
35. Wu YX, Liang D, Wang YH et al. (2013) Correction of a Genetic Disease in Mouse via Use of CRISPR-Cas9[J]. Cell Stem Cell. 2013;13(6):659–662.
36. Taketani Y, Kitamoto K, Sakisaka T et al. (2017) Repair of the TGFBI gene in human corneal keratocytes derived from a granular corneal dystrophy patient via CRISPR/Cas9-induced homology-directed repair[J]. Sci Rep-Uk. 2017;7.
37. Jain A, Zode G, Kasetti RB et al. (2016) CRISPR-Cas9-based treatment of myocilin-associated glaucoma[J]. Proc Natl Acad Sci U S A. 2017;114(42):11199–11204.
38. Bakondi B, Lv WJ, Lui B et al. (2016) In Vivo CRISPR/Cas9 Gene Editing Corrects Retinal Dystrophy in the S334ter-3 Rat Model of Autosomal Dominant Retinitis Pigmentosa[J]. Mol Ther. 2016;24(3):556–563.
39. Latella MC, Di Salvo MT, Cocchiarella F et al. (2016) In vivo Editing of the Human Mutant Rhodopsin Gene by Electroporation of Plasmid-based CRISPR/Cas9 in the Mouse Retina[J]. Mol Ther-Nucl Acids. 2016;5:1–12.
40. Kim K, Park SW, Kim JH et al. (2017) Genome surgery using Cas9 ribonucleoproteins for the treatment of age-related macular degeneration[J]. Genome Res. 2017;27(3):419–426.
41. Zhou T, Benda C, Dunzinger S et al. (2012) Generation of human induced pluripotent stem cells from urine samples[J]. Nat Protoc. 2012;7(12):2080–2089.

42. Miere C, Devito L, Ilic D. (2016) Sendai Virus-Based Reprogramming of Mesenchymal Stromal/Stem Cells from Umbilical Cord Wharton's Jelly into Induced Pluripotent Stem Cells[J]. Methods Mol Biol. 2016;1357:33–44.
43. Ludwig TE, Bergendahl V, Levenstein ME et al. (2006) Feeder-independent culture of human embryonic stem cells[J]. Nat Methods. 2006;3(8):637–646.
44. Ludwig T. J AT. (2007) Defined, feeder-independent medium for human embryonic stem cell culture[J]. Curr Protoc Stem Cell Biol. 2007; Chap. 1: Unit 1C 2.

Figures

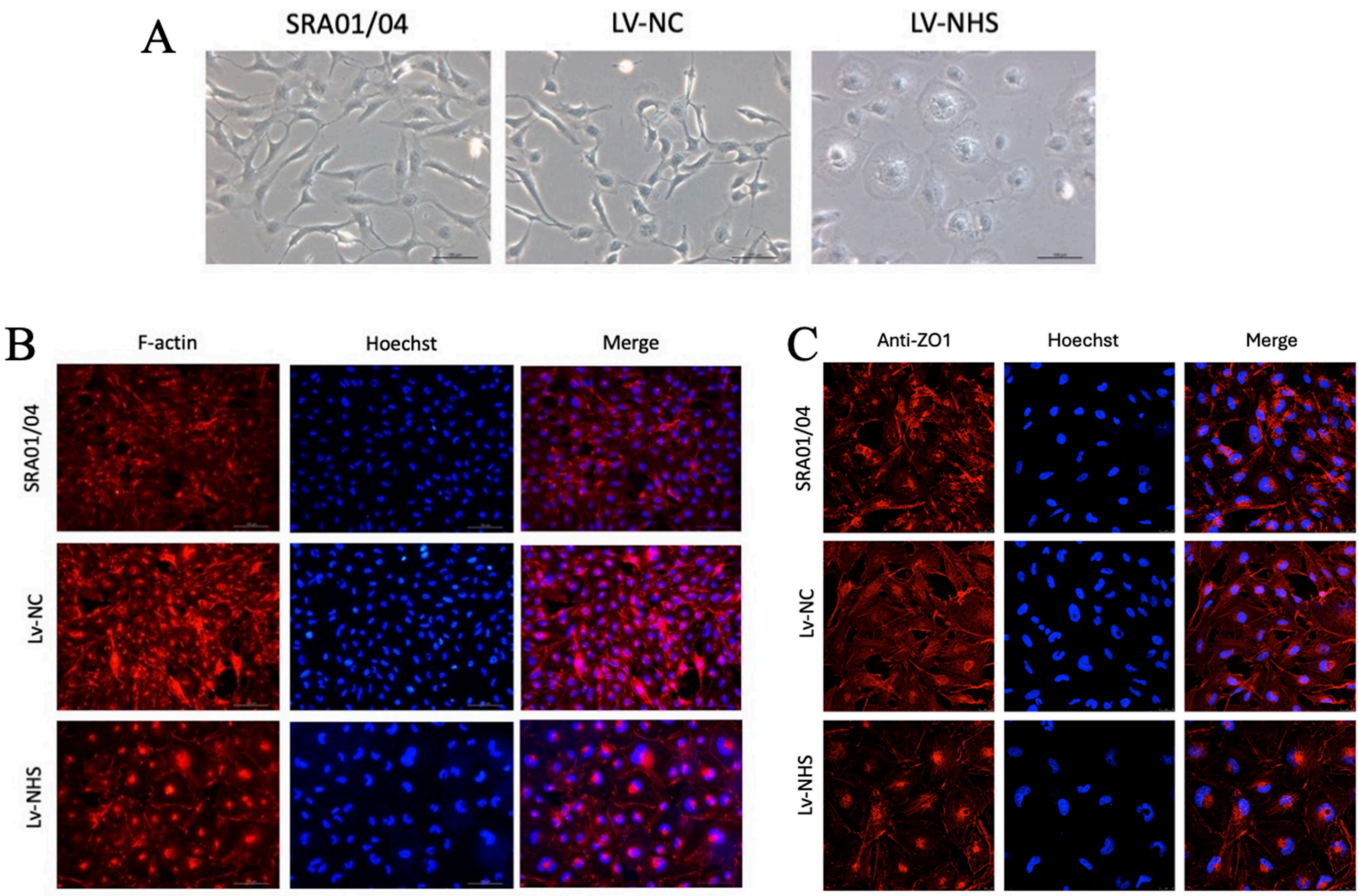


Figure 1

NHS functions in maintaining LEC SRA01/04 cell morphology. A. SRA01/04 cells infected with lentivirus expressing shRNA targeting NHS (LV-NHS) exhibited marked morphological changes compared with WT SRA01/04 cells or cells infected with scramble control RNA (LV-NC). B. F-actin staining by TRITC labeled phalloidin showed reduced amount and irregularly arranged F-actin in LV-NHS cells compared with SRA01/04 and LV-NC cells. C. ZO-1 immunostaining showed reduced amount and abnormal localization of ZO-1 in LV-NHS cells compared with SRA01/04 and LV-NC cells (scale bar, 100 μm).

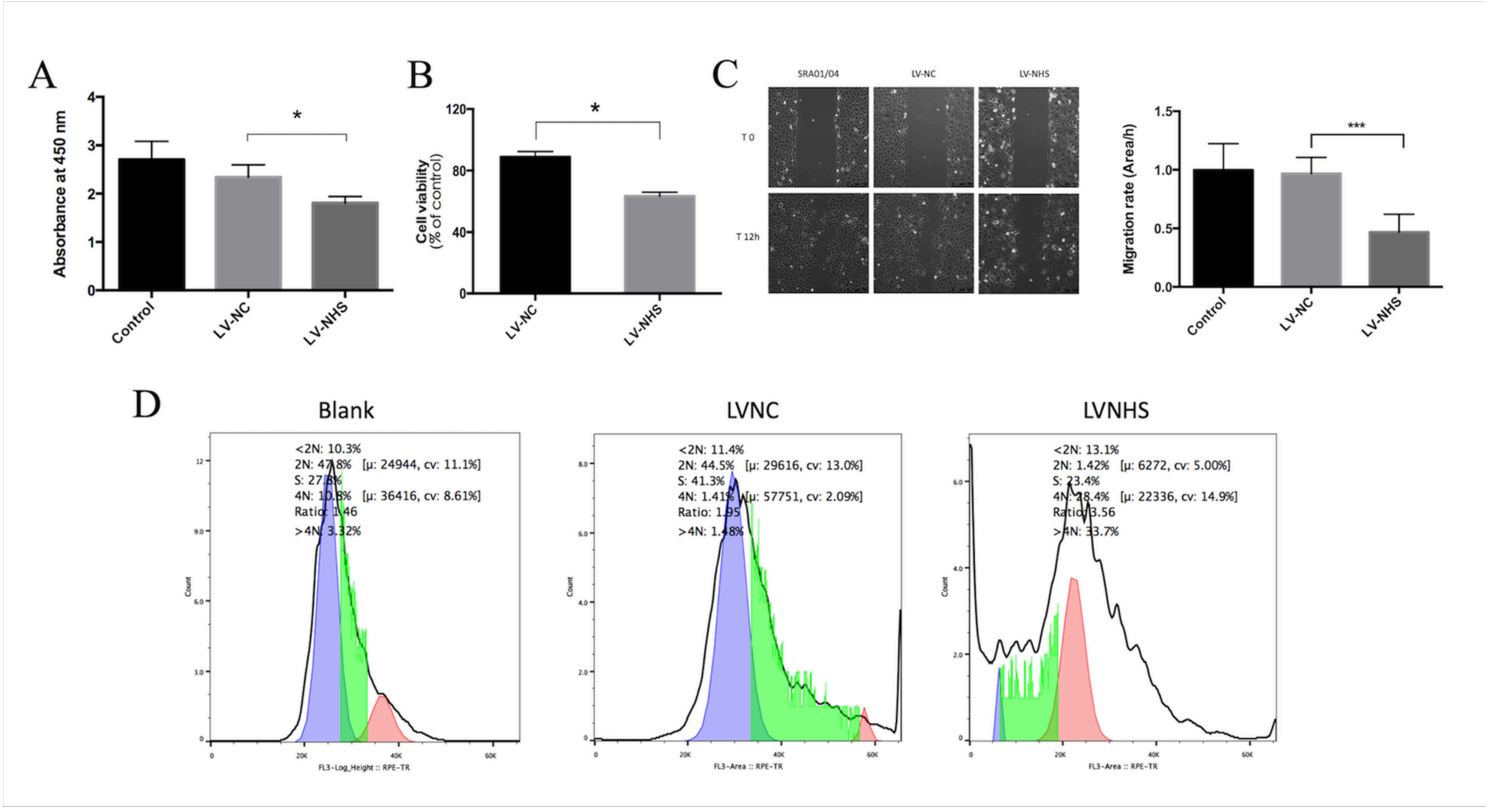


Figure 2

NHS regulates the proliferation, migration, and cell cycle progression of SRA01/04 cells. A, B. CCK-8 assays showed significantly reduced cell proliferation (A) and viability (B) of LV-NHS cells compared with LV-NC cells (*P< 0.05). C. Cell migration assays showed a marked decrease in migration ability following NHS knockdown in LV-NHS as compared to LV-NC cells (***P< 0.001) (scale bar, 250 μm). D. PI staining and flow cytometry analysis showed a significantly decreased G1 peak and greatly increased apoptotic cell population in LV-NHS compared with uninfected SRA01/04 and LV-NC cells. Blue represents G1, green represents S phase, and red represents G2/M phase cells.

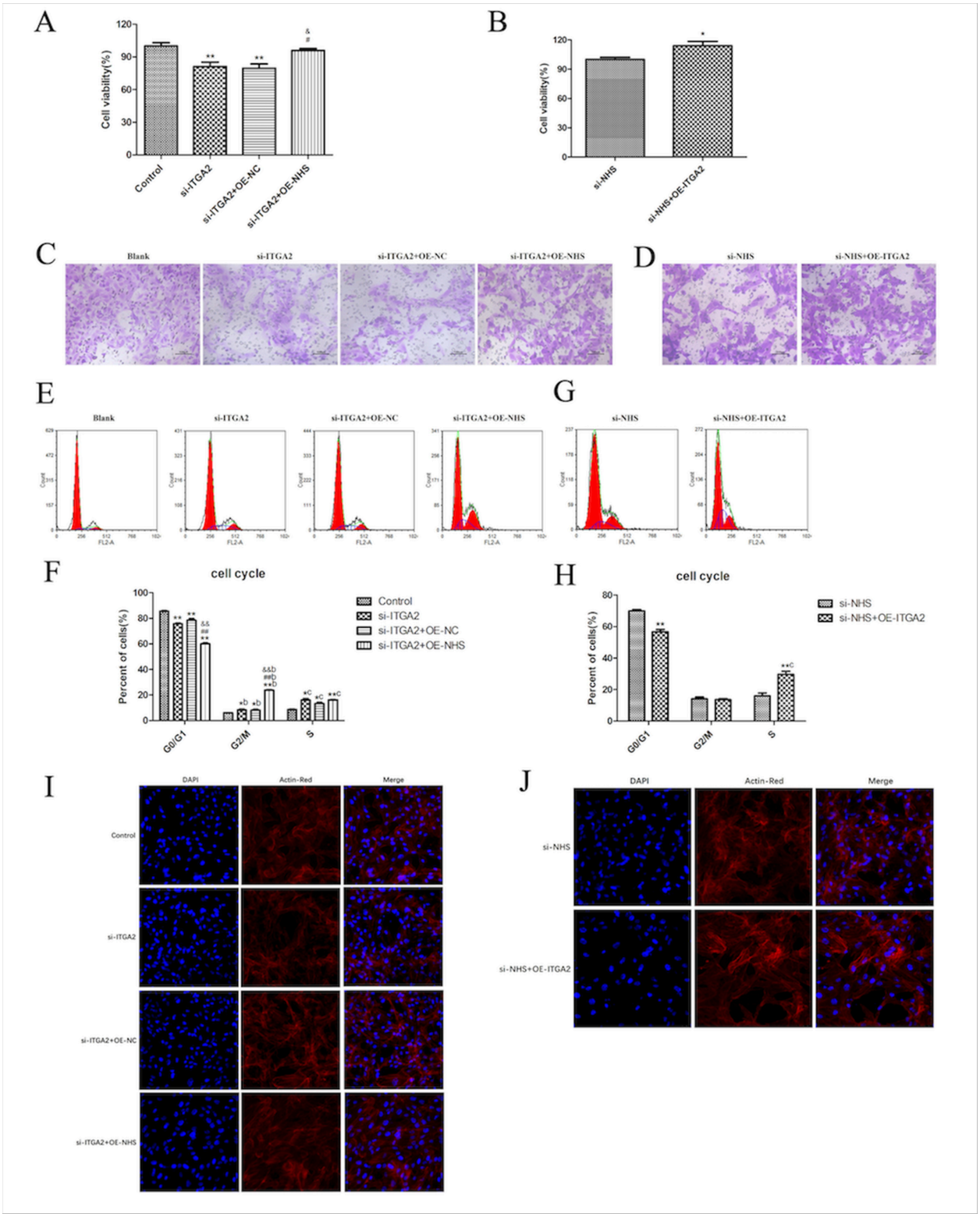


Figure 3

ITGA2 regulates the cell viability, migration, and cell cycle progression of SRA01/04 cells, and the effects caused by ITGA2 deficiency are rescued by NHS overexpression. A. CCK-8 assays showed significantly decreased cell viability of si-ITGA2 cells. Overexpression of NHS (si-ITGA2+OE-NHS) rescued ITGA2 depletion-caused cell viability decrease, while the control overexpression plasmid (si-ITGA2+OE-NC) showed similar cell viability as si-ITGA2. * $P < 0.05$ and ** $P < 0.01$ compared with control;

# *P* < 0.05 compared with si-ITGA2; & *P*< 0.05 compared with si-ITGA2+OE-NC. B. Overexpression of ITGA2 (si-NHS+OE-ITGA2) rescued the NHS depletion (si-NHS)-dependent cell viability decrease. * *P* < 0.05. C. Transwell cell migration assay showed decreased cell migration of si-ITGA2 and si-ITGA2+OE-NC cells compared with blank cells (wild type), which was rescued by overexpression of NHS (si-ITGA2+OE-NHS). D. Transwell cell migration assay showed that overexpression of ITGA2 (si-NHS+OE-ITGA2) increased the cell migration compared with si-NHS. E. Flow cytometry cell cycle analysis of various ITGA2 knockdown cell lines. F. Quantified cell cycle phase analysis of the flow cytometry data in (E). * *P*< 0.05 and ** *P* < 0.01 compared with control; # *P*< 0.05 and ## *P* < 0.01 compared with si-ITGA2; & *P*< 0.05 and && *P* < 0.01 compared with si-ITGA2+OE-NC. G. Flow cytometry cell cycle analysis of various NHS knockdown cell lines. H. Quantified cell cycle phase analysis of the flow cytometry data in (G). ** *P* < 0.01. I. Actin staining in ITGA2 knockdown cells with and without NHS overexpression. J. Actin staining in NHS knockdown cells with and without ITGA2 overexpression.

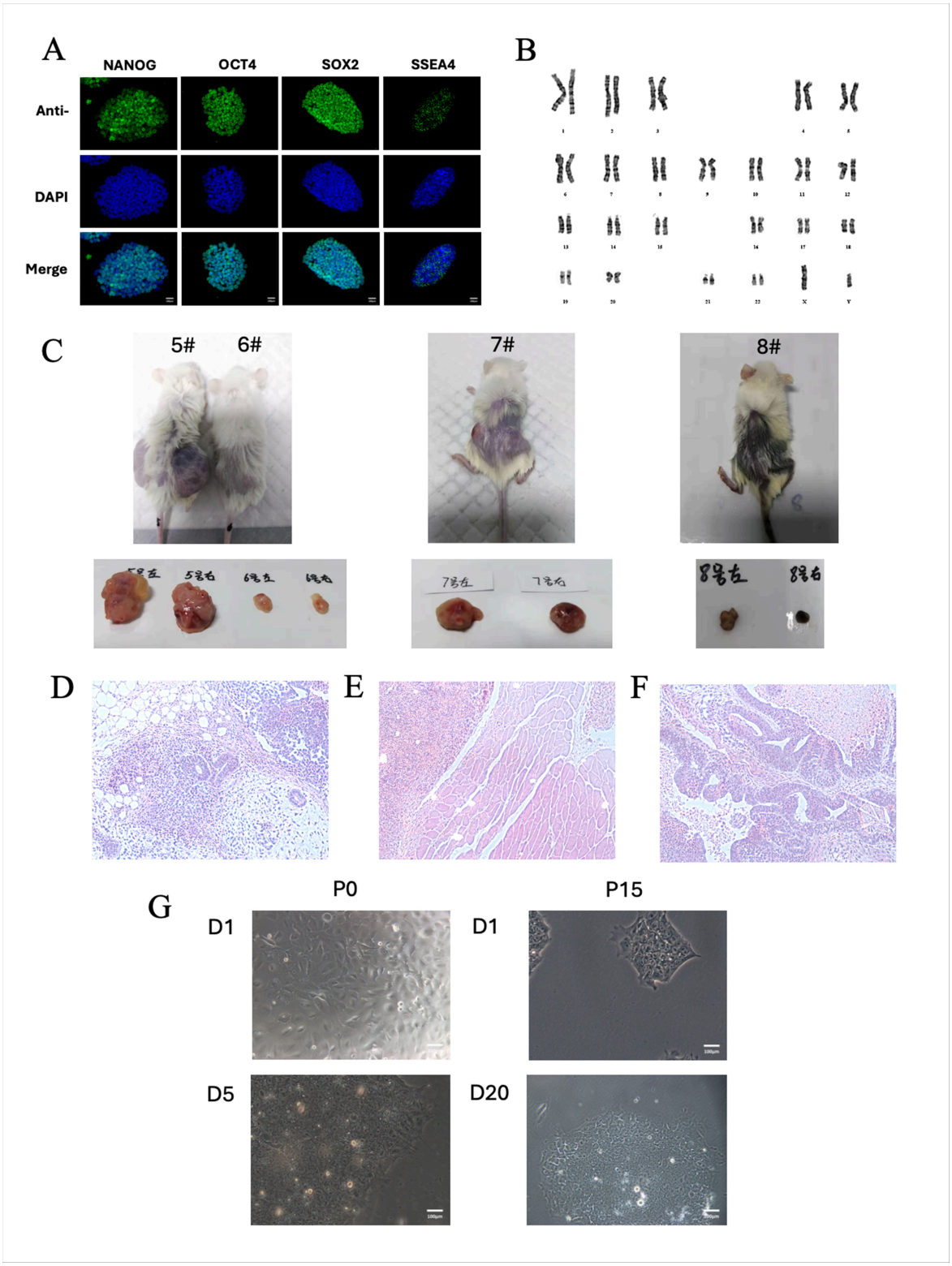


Figure 4

Verification of reprogrammed hiPSCs. A. hiPSCs induced from urine somatic cells were immunofluorescence stained with anti-Nanog, OCT4, Sox2, and SSEA-4 antibodies and DAPI. Images were captured under 20× magnification, and the scale bar represents 100 μm. B. The karyotype of the hiPSCs shows all normal 23 pairs of chromosomes and sex chromosomes of XY. C. Isolated teratomas from mice. Teratomas formed from hiPSCs are significantly smaller than those from H9 cells (#5). D–F.

Histological analyses of the teratomas reveal endoderm (D), mesoderm (E), and ectoderm (F). G. The cell morphology of the 15th generation of hiPSCs is similar to that of the 0th generation.

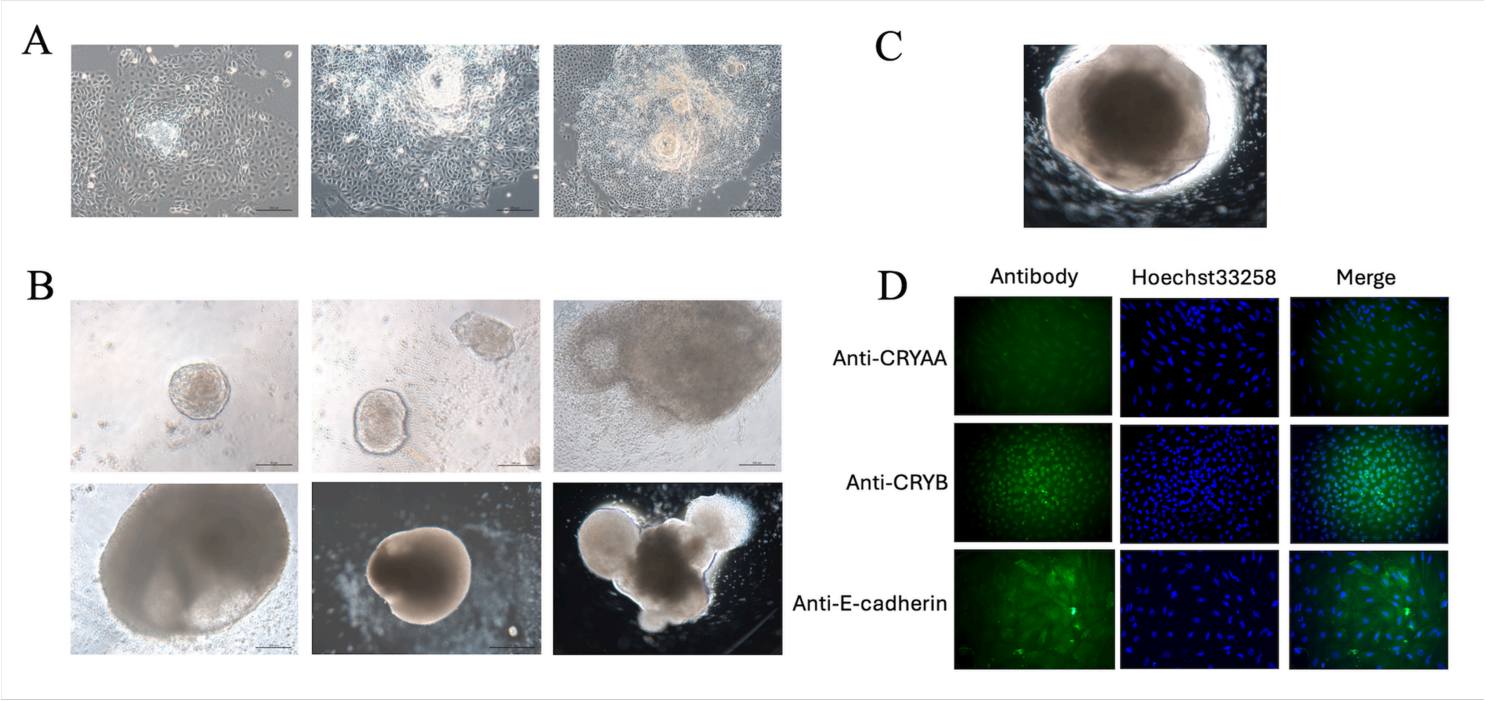


Figure 5

Directed differentiation of hiPSCs into LECs. A. On D11–13 after directed differentiation of the GE-NHS-WT hiPSCs, the cells elongated into a spindle shape and organized into characteristic rose wreath-like structure. From left to right, D11 (scale bar, 200 μm); D12 (scale bar, 200 μm); D12 (scale bar, 500 μm). B, C. In suspension culture, by D25 tissue clusters of approximately 2 mm in diameter were observed. GE-NHS-WT (B) differentiation was observed on D6, D7, D10 (top panel, scale bar, 200 μm), D12, D22, and D25 (bottom panel, scale bar, 500 μm). On D25, peripheral semi-spherical small embryoid bodies formed around the original clusters. On D25, NHS-MT (C) cells showed similar morphology as the GE-NHS-WT cells. D. Differentiated adherent cells on D25 were immunofluorescent stained with anti-CRYAA, CRYA, and E-cadherin. Nuclei were stained with Hoechst. (20× magnitude).

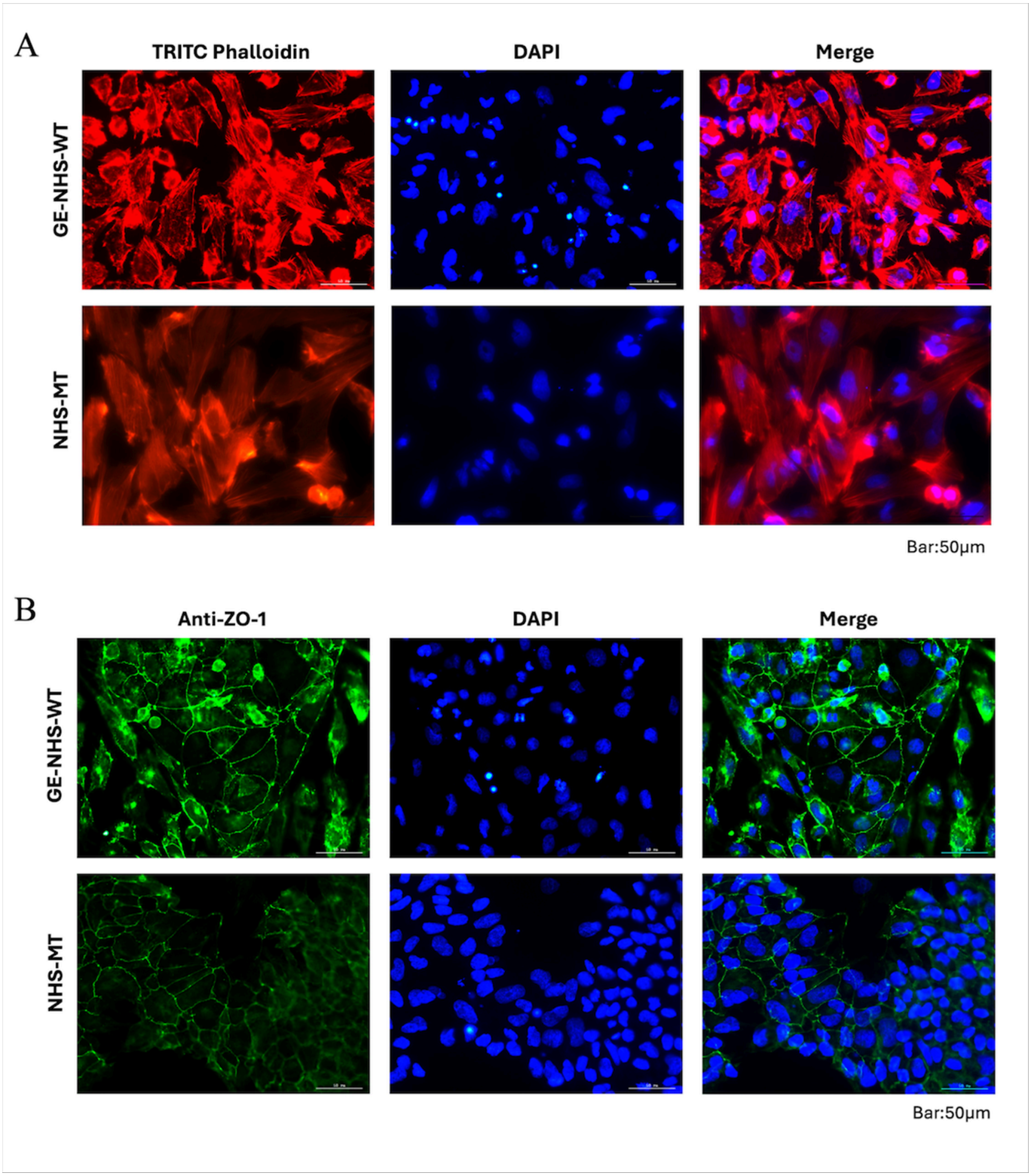


Figure 6

Differentiated NHS-MT cells exhibit cytoskeletal and junctional defects. A. ZO-1 immunostaining assay shows reduced amount and abnormal localization of ZO-1 in NHS-MT cells compared with GE-NHS-WT cells. B. F-actin immunostaining assay shows that the F-actin protein levels were similar in both cell types, while the arrangement of F-actin in NHS-MT was significantly irregular. Nuclei were stained with DAPI (scale bar, 50 μm).

Supplementary Files

This is a list of supplementary files associated with this preprint. Click to download.

- SupFig1.tiff
- SupFig2.tiff
- SupFig3.tiff
- SupFig4.tiff
- SupFig5.tiff
- SupFig6.tiff
- SupFig7.tiff
- Sup.Tables.docx